

Latitudinal and radial gradients of galactic cosmic ray protons in the inner heliosphere – PAMELA and Ulysses observations

N. De Simone¹, V. Di Felice¹, J. Gieseler³, M. Boezio², M. Casolino¹, P. Picozza¹, PAMELA Collaboration[†], and B. Heber³

¹INFN, Structure of Rome “Tor Vergata” and Physics Department of University of Rome “Tor Vergata”, Via della Ricerca Scientifica 1, I-00133 Rome, Italy

²INFN, Structure of Trieste and Physics Department of University of Trieste, I-34147 Trieste, Italy

³Inst. für Experimentelle und Angewandte Physik, Christian-Albrechts-Universität Kiel, Leibnizstr. 11, 24118 Kiel, Germany

Received: 15 November 2010 – Revised: 7 March 2011 – Accepted: 13 April 2011 – Published: 22 September 2011

Abstract. Ulysses, launched on 6 October 1990, was placed in an elliptical, high inclined (80.2°) orbit around the Sun, and was switched off in June 2009. It has been the only spacecraft exploring high-latitude regions of the inner heliosphere. The Kiel Electron Telescope (KET) aboard Ulysses measures electrons from 3 MeV to a few GeV and protons and helium in the energy range from 6 MeV/nucleon to above 2 GeV/nucleon. The PAMELA (Payload for Antimatter Matter Exploration and Light-nuclei Astrophysics) space borne experiment was launched on 15 June 2006 and is continuously collecting data since then. The apparatus measures electrons, positrons, protons, anti-protons and heavier nuclei from about 100 MeV to several hundreds of GeV. Thus the combination of Ulysses and PAMELA measurements is ideally suited to determine the spatial gradients during the extended minimum of solar cycle 23. For protons in the rigidity interval 1.6 – 1.8 GV we find a radial gradient of 2.7%/AU and a latitudinal gradient of -0.024% /degree. Although the latitudinal gradient is as expected negative, its value is much smaller than predicted by current particle propagation models. This result is of relevance for the study of propagation parameters in the inner heliosphere.

adiabatic deceleration in the expanding solar wind. As pointed out by Jokipii et al. (1977) these drift effects should also be an important element of cosmic ray modulation. Models taking these effects into account (Potgieter et al., 2001) predict the latitudinal distribution of galactic cosmic ray (GCR) protons and electrons. In the 1980s and in the 2000s, during an $A < 0$ -solar magnetic epoch, a negative latitudinal gradient for positively charged cosmic rays is predicted. Such gradients were found by the cosmic ray instruments aboard the two Voyagers (Cummings et al., 1987; McDonald et al., 1997a). In the 1970s and 1990s, during an $A < 0$ -solar magnetic epoch, Pioneer and Ulysses measurements in 1974 to 1977 and 1994 to 1995 confirmed the expectation of positive latitudinal gradients (McKibben, 1989; Heber et al., 1996a). In particular, Ulysses measurements during the previous solar minimum have been reported by Heber et al. (1996b) and Heber et al. (1999) using the measurements of the IMP 8 spacecraft as a baseline close to Earth.

In this work the data comparison with PAMELA has been carried out in the period of overlap of the two missions, between July 2006 and July 2009. Because the solar activity changes the GCR intensity in a rigidity dependent way, it is important to compare data samples at the same rigidity. Therefore, after a brief description of the two instruments in Sect. 2, we will use two different methods in Sect. 3 to define the most suitable rigidity range for comparison and we will then calculate the corresponding gradients.

1 Introduction

Energetic charged particles propagating in the heliosphere are scattered by irregularities in the heliospheric magnetic field, undergo gradient and curvature drifts, convection and

2 Instrumentation

The observations presented here were made with the Cosmic and Solar Particle Investigation (COSPIN) Kiel Electron



Correspondence to: N. De Simone
(desimone@roma2.infn.it)

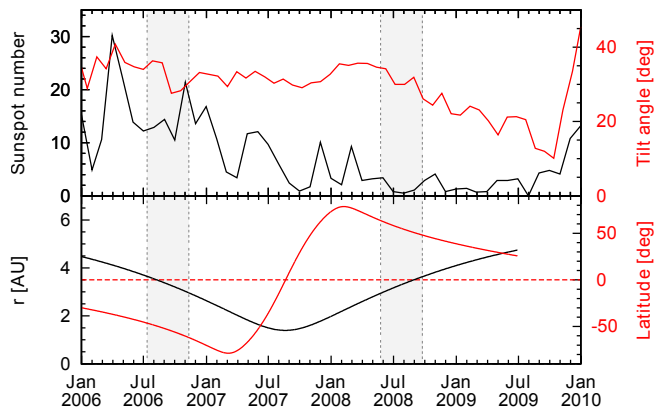


Fig. 1: As a function of time: tilt angle and sunspot number (upper panel), KET heliocentric latitude and radial distance (lower panel). Marked by shading are the comparison intervals used to investigate the temporal variation (see Sect. 3.1).

Telescope (KET) aboard Ulysses (Simpson et al., 1992) between 1.4 and 5 AU and PAMELA apparatus (Picozza et al., 2007) in low Earth orbit.

2.1 The out-of-ecliptic Ulysses mission

The main scientific goal of the joint ESA-NASA Ulysses deep-space mission was to make the first-ever measurements of the unexplored region of space above the solar poles. The GCR intensity measured along the Ulysses orbit results from a combination of temporal and spatial variations. Ulysses was launched first towards Jupiter. Following the fly-by of Jupiter in February 1992, the spacecraft has been traveling in an elliptical, Sun-focused orbit inclined at 80.2 degrees to the solar equator. The characteristics of the Ulysses trajectory after January 2006, during the declining phase of solar cycle 23, are displayed in the lower panel of Fig. 1. The upper panel of that figure shows the sunspot number (black curve) and tilt angle (red curve), respectively, indicating a period of several years of very low solar activity. Marked by shading are two periods after the launch of the PAMELA spacecraft in October 2006 and July 2008 when Ulysses was at about 3.5 AU and 50°. The polar passes are defined to be those periods during which the spacecraft is above 70 degrees heliographic latitude in either hemisphere. Beginning of 2007, the spacecraft reached a maximum southern latitude of 80° at a distance of 2.3 AU. The spacecraft then performed a whole latitude scan of 160° within 11 months. On 30 June 2009, at the minimum of the solar cycle, Ulysses was switched off on its way returning towards the heliographic equator at a radial distance of 5.3 AU.

2.2 Ulysses Kiel electron telescope

The KET measures protons and α -particles in the energy range from 6 MeV/n to above 2 GeV/n, and electrons in the

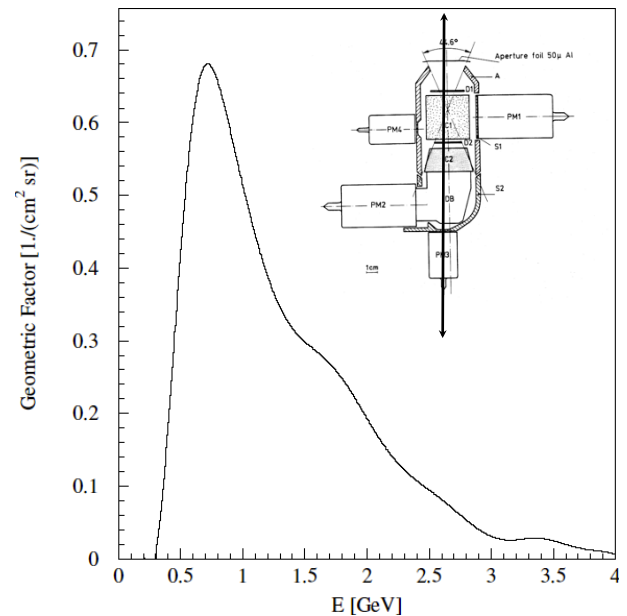


Fig. 2: Energy dependent geometric factor of one of the KET proton channels (Gieseler et al., 2010). The inset shows a sketch of the KET (from Simpson et al., 1992).

energy range from 3 MeV to some GeV. For a complete description of the KET instrument see Simpson et al. (1992). Using a GEANT-3 simulation of the Kiel Electron Telescope (Gieseler et al., 2010), its geometrical factor for different energy ranges can be determined. As an example, the energy dependent response of the channel between 500 MeV and 1400 MeV is displayed in Fig. 2 (the inset displays a sketch of the sensor). It is important to note that in the energy range of interest both forward and backward penetrating particles contribute to the measurements.

2.3 The PAMELA detector

PAMELA is designed to perform high-precision spectral measurement of charged particles of galactic, heliospheric and trapped origin over a wide energy.

PAMELA was mounted on the Resurs DK1 satellite launched on an elliptical and semi-polar orbit, with an altitude varying between 350 km and 600 km, at an inclination of 70°. At high latitudes, the low geomagnetic cutoff allows low-energy particles (down to 50 MeV) to be detected and studied.

The apparatus comprises a number of high performance detectors, capable of identifying particles through the determination of charge (Z), rigidity ($R = pc/|Ze|$, p being the momentum of a particle of charge $Z \cdot e$) and velocity ($\beta = v/c$) over a wide energy range. The device is built around a permanent magnet with a six-plane double-sided silicon micro-strip tracker, providing absolute charge information and track-deflection ($\eta = \pm 1/R$, with the sign de-

pending on the sign of the charge derived from the curvature direction) information. A scintillator system, composed of three double layers of scintillators (S1, S2, S3), provides the trigger, a time-of-flight measurement and an additional estimation of absolute charge. A silicon-tungsten imaging calorimeter, a bottom scintillator (S4) and a neutron detector are used to perform lepton-hadron discrimination. An anti-coincidence system is used off-line to reject spurious events generated by particles interacting in the apparatus. A more detailed description of PAMELA and the analysis methodology can be found in Casolino et al. (2008).

3 Data analysis

For our analysis we assume that in the inner solar system the variation of the cosmic ray flux is separable in time and space (McDonald et al., 1997b). Let $J_U(R, t, r, \theta)$ and $J_E(R, t, r_E, \theta_E)$ be the flux intensities at rigidity R and time t averaged over one solar rotation and measured by Ulysses KET along its orbit and PAMELA at Earth, respectively. Then:

$$J_U(R, t, r, \theta) = J_E(R, t, r_E, \theta_E) \cdot f(R, \Delta r, \Delta \theta) \quad (1)$$

where $f(R, \Delta r, \Delta \theta)$ is a function of the rigidity R and of the heliospheric radial (Δr) and latitudinal ($\Delta \theta$) distances between the two spacecraft. The radial distance Δr is determined by:

$$\Delta r = r_U - r_E. \quad (2)$$

Although Heber et al. (1996b) and Simpson et al. (1996) found a small asymmetry of the GCR flux with respect to the heliographic equator, we assume that the proton intensity is symmetric. Thus, the latitudinal distance $\Delta \theta$ is determined by:

$$\Delta \theta = |\theta_U| - |\theta_E|. \quad (3)$$

In both formulas U and E indicate the spatial positions of Ulysses and Earth, respectively.

Assuming that latitudinal and radial variations are separable and that the variation in r (see Eq. (2)) and θ (see Eq. (3)) can be approximated by an exponential law, Eq. (1) can be rewritten as:

$$J_U(R, t, r, \theta) = J_E(R, t, r_E, \theta_E) \exp(G_r \cdot \Delta r) \exp(G_\theta \cdot \Delta \theta) \quad (4)$$

where, G_r and G_θ are the rigidity dependent (Cummings et al., 1987; Fujii and McDonald, 1999; Heber et al., 1996a; McDonald et al., 1997a; McKibben, 1989) radial and latitudinal gradients, respectively.

3.1 Determination of the mean rigidity through temporal variation

In order to use Eq. (4) to estimate the gradients, we need to define the rigidities R for the comparison, taking into account the rigidity dependent geometric factor of the KET channel.

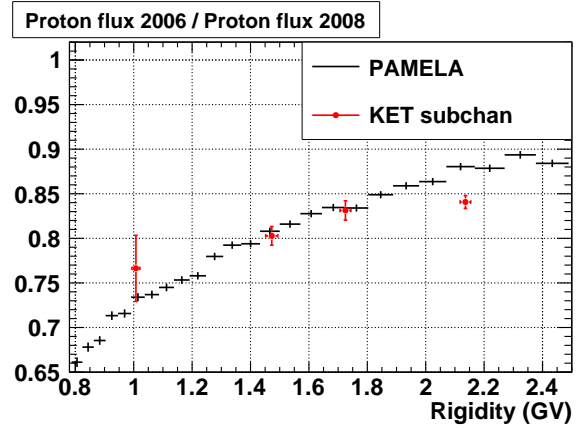


Fig. 3: Rigidity dependence of the rate of increase as defined in Eq. (5). In black the ratio between the PAMELA differential flux intensities in 2006 and in 2008 as a function of the rigidity measured by the spectrometer. The same ratio is indicated by the red symbol for the KET channels, obtained using Eq. (6), the simulated response function and the shape of the differential flux measured by PAMELA. The KET channel at rigidity ~ 1.7 GV has been selected for this analysis.

We will now discuss a method that takes advantage of the high rigidity resolution ($< 5\%$ in the region of interest) provided by the PAMELA magnetic spectrometer (Picozza et al., 2007), and we will use it as a calibration tool to find the KET channels that show a mean rigidity in good agreement with PAMELA.

Let t_1 be a time for which KET is in the southern hemisphere at a radial distance r_1 and at a latitude θ_1 , and t_2, r_2, θ_2 the respective for the northern hemisphere (see periods in Fig. 1). By choosing t_1 and t_2 so that $r_1 \approx r_2$ and $\theta_1 \approx \theta_2$, and considering that, consequently, $f(R, \Delta r, \Delta \theta)$ is approximately the same at t_1 and t_2 , it follows that:

$$\frac{J(R, t_1, r_1, \theta_1)}{J(R, t_2, r_2, \theta_2)} = \frac{J(R, t_1, r_E, \theta_E)}{J(R, t_2, r_E, \theta_E)}. \quad (5)$$

KET PAMELA

In this way the effect of spatial gradients cancels out and the flux variation between time t_1 and time t_2 measured by KET (left side of Eq. (5)) can be compared with the flux variation measured at Earth by PAMELA (right side of Eq. (5)). Since the temporal recovery is rigidity dependent, the same flux variation can only be obtained if the mean rigidity of the KET channel is the same as the one by PAMELA. This is illustrated in Fig. 3: first we determined the proton intensities in the time intervals from 10 July 2006 to 7 November 2006 (t_1) and from 24 May 2008 to 21 September 2008 (t_2), when Ulysses was at nearly the same latitude and radial distance to the Sun. No ad hoc corrections are applied to the KET data. The black and red symbols correspond to the intensity ratios

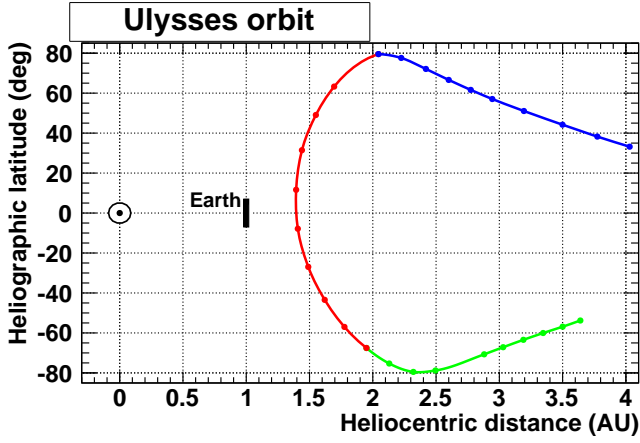


Fig. 4: Ulysses heliographic latitude as a function of radial distance. Three different phases in the trajectory have been marked by different colors: Red indicates the fast latitude scan, and green and blue the slow ascent and descent in the southern and northern hemisphere, respectively. The Earth is located between 0.98 and 1.02 AU and between -7° and 7° with respect to the heliographic equator.

between the 2006 and 2008 period using the PAMELA and KET measurements, respectively, as a function of particle rigidity. The PAMELA observation confirms the expectation that the higher the rigidity the smaller the increase in time.

The mean rigidity of a KET channel, $\langle R \rangle_{\text{KET}}$, can be obtained in two ways:

- As a first approach (*method a*), we make use of the KET geometrical factor $GF_{\text{KET}}(R)$, as calculated in Gieseler et al. (2010), and derive:

$$\langle R \rangle_{\text{KET}}(t) = \frac{\int dR J_{\text{PAM}}(R, t) \cdot GF_{\text{KET}}(R) \cdot R}{\int dR J_{\text{PAM}}(R, t) \cdot GF_{\text{KET}}(R)} \quad (6)$$

where $J_{\text{PAM}}(R, t)$ is the differential flux measured by PAMELA at the rigidity R and time t . We define the mean rigidity of the KET points of Fig. 3 and calculate the associated uncertainties, taking into account the variation of the proton flux due to the solar modulation, as follows:

$$\overline{\langle R \rangle_{\text{KET}}} = \frac{1}{2} \left| \langle R \rangle_{\text{KET}}(t_1) + \langle R \rangle_{\text{KET}}(t_2) \right|$$

$$\delta \overline{\langle R \rangle_{\text{KET}}} = \frac{1}{2} \left| \langle R \rangle_{\text{KET}}(t_1) - \langle R \rangle_{\text{KET}}(t_2) \right|$$

From the plot it follows that for most of the KET channels we get a reasonable agreement with PAMELA, indicating that both instruments respond to temporal variation of the same particle population.

However, the best agreement is found at a mean rigidity of (1.73 ± 0.02) GV, according to the integral average in Eq. (6).

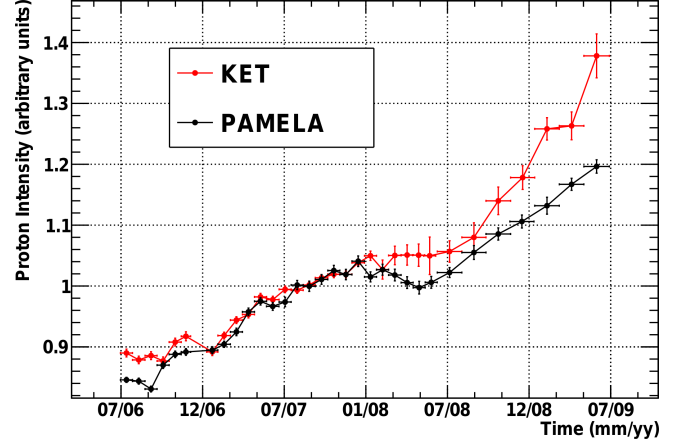


Fig. 5: 54-day averaged intensities (arbitrary units) of ~ 1.7 GV protons as measured by the KET instrument aboard Ulysses (red curve) and by PAMELA (black curve). The two curves are scaled to match at the time of Ulysses' closest approach to Earth in August 2007.

- Alternatively (*method b*), we can also find the PAMELA rigidity interval for the comparison as the range where data from both spacecraft show a compatible variation 2006/2008. The value found for the KET channel under discussion is (1.68 ± 0.10) GV, consistent with the previous one. Both intervals will be considered in the following.

3.2 Calculation of the spatial gradients

The orbits of Ulysses and the Earth are known and provide the heliospheric radial (Δr) and latitudinal ($\Delta \theta$) distances between Ulysses and PAMELA. In Fig. 4, Ulysses latitude is shown as a function of radial distance: in red the fast latitude scan of Ulysses going from the southern to the northern hemisphere is indicated. Green and blue mark the slow ascent and descent in the southern and northern hemisphere, respectively.

In order to calculate the spatial gradients, Eq. (4) can be written in the form:

$$\log\left(\frac{J_U}{J_E}\right) = G_r \cdot \Delta r + G_\theta \cdot \Delta \theta$$

$$\underbrace{\log\left(\frac{J_U}{J_E}\right) / \Delta r}_{:=Y} = G_r + G_\theta \cdot \underbrace{\frac{\Delta \theta / \Delta r}_{:=X}} \quad (7)$$

where $X := \Delta \theta / \Delta r$ and $Y := \log(J_U / J_E) / \Delta r$. If G_r and G_θ were independent of time and space, their values would be simply given by the offset and the slope of a straight line. It is important to recall that Eq. (7) holds only if the data from KET and PAMELA refer to the same rigidity.

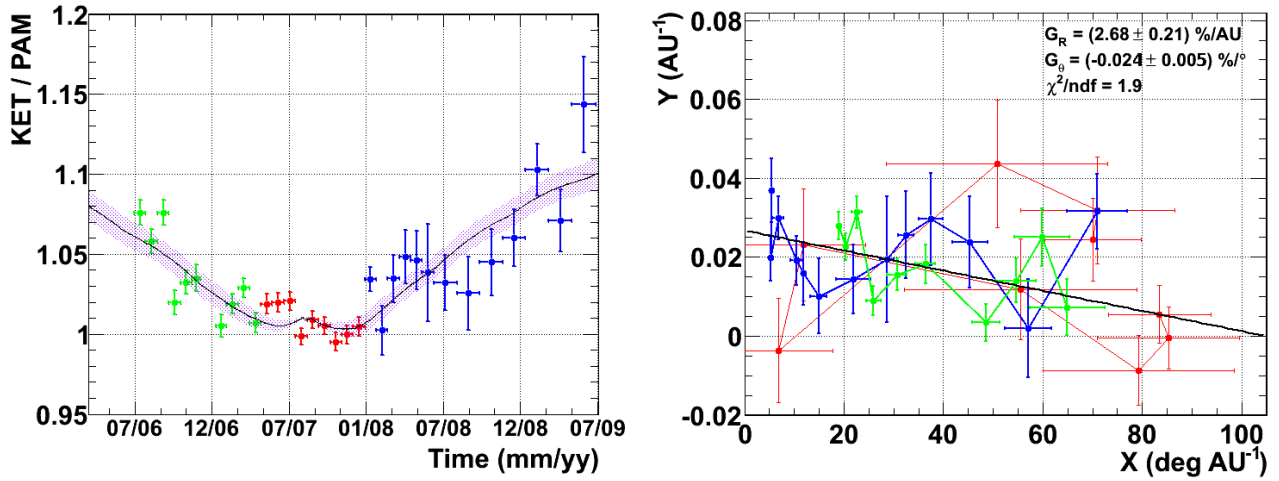


Fig. 6: Left: Ulysses (J_U) and PAMELA (J_E) intensity ratio as a function of time. PAMELA intensities have been calculated by using the measured intensity spectrum at Earth folded with the simulated response function of KET (see Fig. 2), as described in Eq. (8). The right panel displays the 54-day averaged Y as a function of X . The black line represents the result of a linear fit with a radial and latitudinal gradient of $G_R = (2.7 \pm 0.2)\%/AU$ and $G_\theta = (-0.024 \pm 0.005)\%/degree$, respectively. As in Fig. 4, the three different phases in the trajectory have been marked by different colors.

While during the fast latitude scan X varies strongly within a 54-day averaging period, it is well defined during the slow descent and ascent period. We will make use of these colors in order to check our results for consistency in the northern and southern hemisphere, which would be reflected in the Y versus X plot.

In the following we will determine the parameters G_R and G_θ comparing the given KET channel with the PAMELA data selected using the two alternative methods described in Sect. 3.1. In order to minimize the uncertainties in the estimation of the flux intensities of the KET instrument, potentially connected to the absolute determination of the geometrical factor, we adopt a normalization of the time profiles at the closest approach of Ulysses to Earth, in August 2007. For this purpose, an iterative method has been applied, that will be described in detail in Appendix A.

Method a)

The intensity time profile at Earth, $J_E(t)$, is calculated by weighting the measured PAMELA energy spectra with the response function of the KET channel as displayed in Fig. 2:

$$J_E(t) \propto \int dR J_{PAM}(R, t) \cdot GF_{KET}(R), \quad (8)$$

where $J_{PAM}(R, t)$ is the differential intensity measured by PAMELA at the rigidity R and at the time t . The time history of both the KET and the weighted PAMELA channel are shown in Fig. 5. Although in 2007 and 2008 the lowest sunspot numbers have been obtained since the beginning of space age, the cosmic ray flux in the rigidity range below 2.5 GV has not recovered (Heber et al., 2009).

The intensity time profile ratio J_U/J_E is displayed in Fig. 6 left, while Y as a function of X , as determined by Eq. (7), is displayed on the right. Accordingly to Fig. 4, the three different phases in the trajectory segments have been marked by different colors. The black line through the data points represents the linear fit which gives the latitudinal gradient G_θ as the slope and the radial gradient G_R as the intercept with the Y-axis. The iterative algorithm (see Appendix A) converges after four iteration steps, as shown by Fig. 10, independently of the starting conditions, indicating the robustness of our method.

The results are:

$$\begin{aligned} G_R &= (2.7 \pm 0.2) \% / AU \\ G_\theta &= (-0.024 \pm 0.005) \% / degree \end{aligned} \quad (9)$$

Method b)

The gradients can also be determined without considering the simulated response function of KET. As discussed in Sect. 3.1 and shown in Fig. 3, the intensity of the PAMELA proton flux in the rigidity range (1.68 ± 0.10) GV has the same temporal increase as the KET channel under analysis. By selecting PAMELA protons in this rigidity range, we get the gradients:

$$\begin{aligned} G_R &= (2.6 \pm 0.3) \% / AU \\ G_\theta &= (-0.023 \pm 0.008) \% / degree \end{aligned} \quad (10)$$

These values are consistent with the values of *method a)*, indicating that the simulated response function of the KET channel leads to systematic uncertainties smaller than the estimated errors on the gradients.

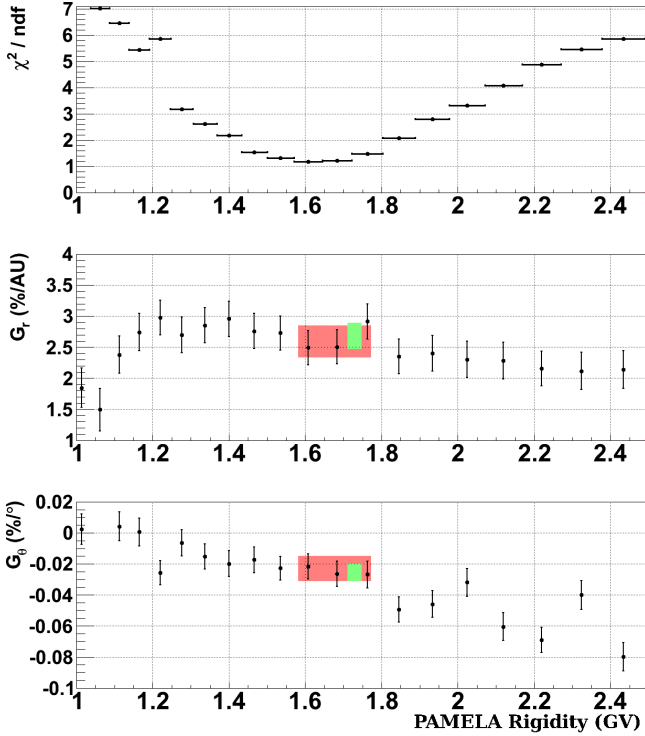


Fig. 7: χ^2 quality parameter (top panel) of the fit of Eq. (7) to the data, radial (middle panel) and latitudinal gradient (bottom panel), as a function of PAMELA rigidity R . A minimum of χ^2 is present in the rigidity interval between $R = 1.54$ GV and $R = 1.72$ GV. While the value of the radial gradient is nearly independent of the rigidity interval, the latitudinal gradient is varying from 0%/degree to $-0.06\%/degree$. Marked by shading are the results for the radial and latitudinal gradient as described in the previous section, showing a good agreement between the two methods described in Sect. 3.2. See text for more details.

3.2.1 The χ^2 -minimization

In what follows, we validate the robustness of the analysis described in the previous section: we calculate the spatial gradients by using the measurements by the PAMELA detector in several small rigidity bins. The quality of the best fit is expected to vary with rigidity. As discussed in Sect. 3.1, Eq. (4) is expected to correctly describe the $\frac{J_U(t)}{J_E(R,t)}$ only at the right mean rigidity R .

Figure 7, top panel, shows that an absolute minimum is present in the χ^2 -distribution around 1.7 GV, consistent with the previous estimations. The values for the radial gradients (middle panel) and latitudinal gradients (bottom panel) are also compatible with the values in Eq. (9) (green area) and Eq. (10) (red area). Furthermore, around the minimum the values of the gradients do not significantly change for small variations in the estimated mean rigidity.

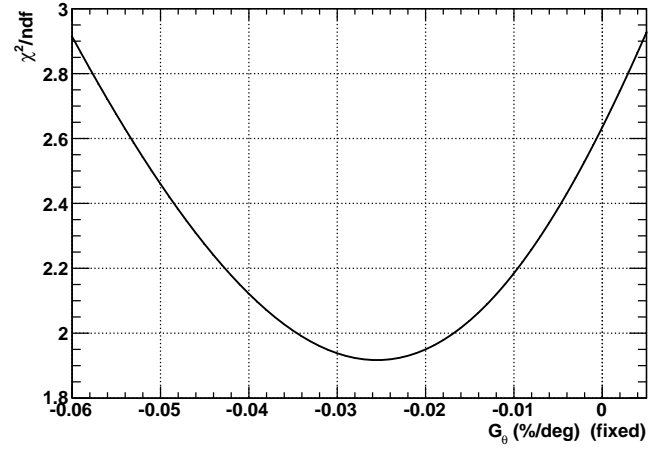


Fig. 8: χ^2/ndf of the fit obtained for different fixed value of G_θ .

4 Summary and conclusions

The Ulysses mission has contributed significantly to the understanding of the major cosmic ray observations in the inner heliosphere and at high heliolatitudes. The first major challenge was that the latitudinal gradients for cosmic ray protons at all energies, but especially at low energies (< 100 MeV), were observed significantly smaller than predicted by drift models for an $A < 0$ -solar magnetic epoch. It became quickly evident that this was due to the overestimation of drifts in the polar regions of the heliosphere and to a too simple geometry for the heliospheric magnetic field. The extension of the mission and the launch of the PAMELA detector in 2006 allowed to perform the comparative analysis illustrated in this work and to determine the radial and latitudinal gradient during an $A < 0$ -solar magnetic epoch.

The analysis has been proven to be robust in several ways: 1) the rate of increase from 2006 to 2008, determined by the KET and the PAMELA instrument independently, agrees very well at the considered rigidity; 2) by varying the mean rigidity between 1.0 GV and 2.5 GV, the best representation of the spatial variation leads to the smallest χ^2 if a mean rigidity about 1.7 GV is chosen; 3) both the radial and latitudinal gradient do not strongly vary with the mean rigidity in the interval of interest.

Thanks to the large geometric factor and high precision measurements of the PAMELA instrument, we could show here that:

1. the mean rigidity comes to be 1.6 – 1.8 GV independently of the method chosen,

therefore we conclude that the simulated response function is reliable and the results of *method a*) can be taken:

2. the radial gradient during the 2000 $A < 0$ -solar magnetic epoch is $(2.7 \pm 0.2)\%/AU$

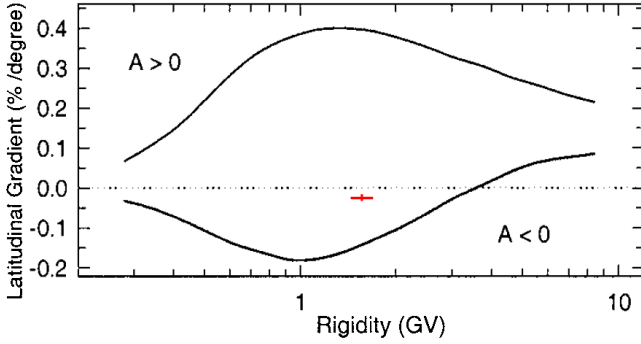


Fig. 9: Computed latitudinal gradients for protons during the past $A < 0$ -solar minimum and the prediction for the current $A < 0$ -solar minimum (see Potgieter et al., 2001). Marked by red point is the latitudinal gradient found in this study.

3. the latitudinal gradient during the same period is only $(-0.024 \pm 0.005)\%/degree$.

Although the absolute error of the uncertainty for the latitudinal gradients looks very small, it is about 20% of the observed value. However, the data are not statistically consistent with a null latitudinal gradient. Applying Student’s t-test (Eadie et al., 1971) to the data, the hypothesis of a null latitudinal gradient is rejected at 99.6% C.L. The gradients lie within the following 95% C.L. intervals: $G_\theta = (-0.0255 \pm 0.0182)\%/degree$ and $G_r = (-2.68 \pm 0.42)\%/AU$. In Fig. 8 we additionally report the χ^2 value of the fit obtained by changing a fixed value of the latitudinal gradient: as expected, the best fit minimizes the χ^2 at $G_\theta \approx -0.024\%/degree$.

In order to estimate the impact of varying solar activity we fitted function in Eq. (7) to the ratios using the period for the slow ascend south, the fast latitude scan and the slow descend north, separately. The values are summarized in Table 1 and vary between 2.5%/AU and 3.1%/AU and $-0.022\%/degree$ and $-0.039\%/degree$, indicating a trend with solar activity cycle to become smaller for solar minimum. However, since the deviation from the mean value of 2.7%/AU and $-0.026\%/degree$ is smaller than one sigma, we randomly chose 20 points out of the full data set of 32 points and calculated the gradients for this subset 10^5 times. The mean of all these values is given in the lowest row.

Our analysis clearly reveals that for the period from 2006 to 2009, close to solar minimum in an $A < 0$ -solar magnetic epoch,

1. the radial gradient is positive as expected. However, it is smaller than previously reported values (e.g. McDonald et al., 1997a).
2. the latitudinal gradient is negative and much smaller than the ones observed in the previous $A < 0$ -solar magnetic epoch (Cummings et al., 1987; McDonald et al., 1997a).

Table 1: The first four rows report the values of the gradients obtained by selecting different time periods. The last row reports the mean and standard deviation of the distribution of values obtained by randomly selecting 10^5 times a subsample of 20 points out the full data set of 32 points.

Data set	$G_r(\%/ AU)$	$G_\theta(\%/ deg)$	χ^2 / ndf
All data	2.67 ± 0.21	-0.026 ± 0.006	1.98
South pole (green)	3.10 ± 0.38	-0.039 ± 0.011	3.32
Fast latitude scan (red)	3.01 ± 1.18	-0.026 ± 0.016	2.52
North pole (blue)	2.53 ± 0.36	-0.022 ± 0.017	1.04
Statistical sub-sampling (20 points over 32)	2.6 ± 0.3	-0.025 ± 0.006	

Figure 9 from Potgieter et al. (2001) displays the calculated rigidity dependence of the non-local latitudinal gradient. The parameters for this calculations are optimized to reproduce the measurements from Heber et al. (1996b) for the fast latitude scan in 1994 to 1995 during an $A < 0$ -solar magnetic epoch (see also Burger et al., 2000). The prediction shown by the lower curve for the $A < 0$ -magnetic epoch are based on the same set of parameters but opposite magnetic field polarity. In contrast to their calculations, the absolute value of the latitudinal gradient found is much lower. There are several processes which may account for the observed discrepancy:

- The measured solar wind parameters, wind pressure and magnetic field strength are much lower than in the previous solar cycle (McComas et al., 2008; Smith and Balogh, 2008). Thus the size of the modulation volume as well as the diffusion tensor will be different (e.g. Ferreira et al., 2003)
- As stated in Potgieter et al. (2001), drift effects depend on the maximum latitudinal extent of the heliospheric current sheet (tilt angle). Although the magnetic field strength was much lower than in the previous solar magnetic minima, the tilt angle was much higher (e.g. Heber et al., 2009).
- The diffusion coefficients may depend on the heliospheric magnetic field polarity (Ferreira and Potgieter, 2004).

In order to contribute to our understanding on how the Sun is modulating the galactic cosmic ray flux and especially to support theoretical studies of the propagation parameters in

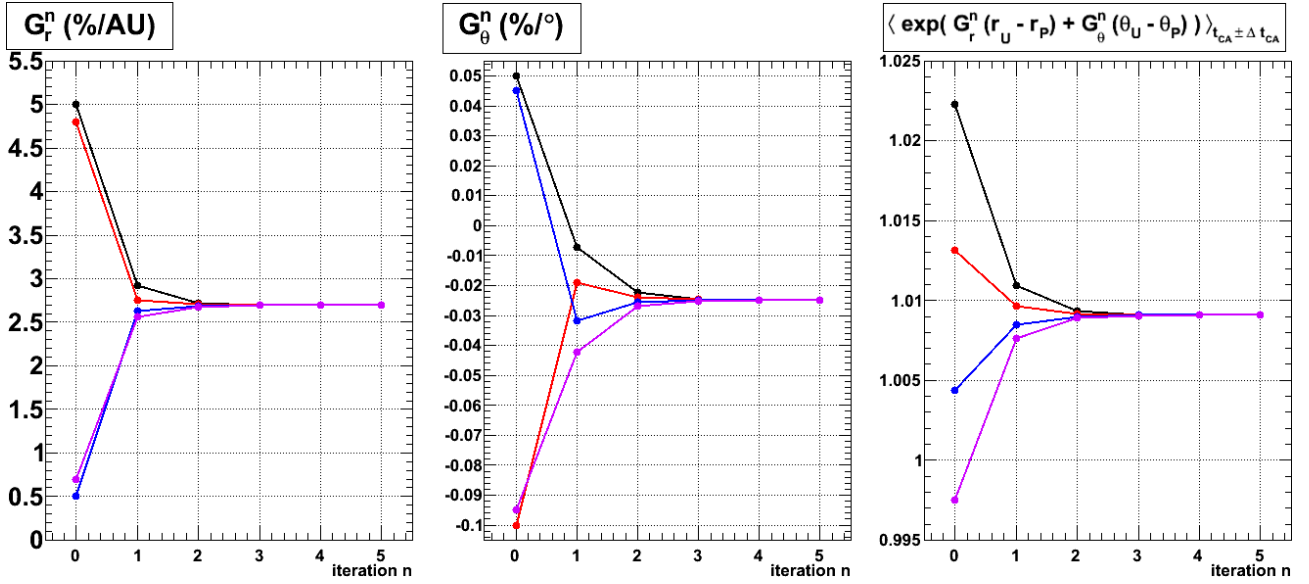


Fig. 10: Radial and latitudinal gradients as well as the normalized intensity ratio at the closest approach as a function of the number of iteration. When the radial and the latitudinal gradients change less than 0.002% from one step to the next we stop the procedure. The minimization is performed using the code MINUIT (James and Roos, 1975).

the inner heliosphere (Shalchi et al., 2010; Minnie et al., 2007; Burger et al., 2000), detailed calculations and further analysis of the Ulysses and PAMELA data are necessary. From the latter we will obtain the radial and latitudinal gradient at other rigidities between several 100 MV and a few GV.

Appendix A

In the following we will describe the iterative method that allows us to minimize the uncertainties in the estimation of the ratio J_U/J_E due to the systematic in our knowledge of J_U . This is necessary for the measurement of the spatial gradients G_r and G_θ according to Eq. (7). We will show this method as applied to the rigidity range defined for the *method a*).

We start with arbitrary spatial gradients $G_r^{k=0}$ and $G_\theta^{k=0}$ (where k is the iteration step index) chosen in the range of findings in the 1980s and 1990s (Heber et al., 2008; Fujii and McDonald, 1999). We use them to determine a normalization that is for each step k defined by:

$$\frac{J_U}{J_E} \Big|_N^k := \sum_{i=1}^n \frac{\exp(G_r^{k-1} \cdot \Delta r_i) \cdot \exp(G_\theta^{k-1} \cdot \Delta \theta_i)}{n}, \quad (\text{A1})$$

with $n = 27$ the number of days in the normalization interval N , in August 2007, Δr_i and $\Delta \theta_i$ the according daily values of the trajectory data. By using this in Eq. (7), we derive successive approximations of the spatial gradients. After a few iterations, this method converges and delivers the final normalization and spatial gradients. In the first step of our iterative method the normalization $\frac{J_U}{J_E} \Big|_N$ of KET and PAMELA

intensities as a function of time has been calculated by using different radial and latitudinal gradients (see Eq. (A1)). The corresponding values for Y are calculated by using Eq. (7). By fitting Eq. (7) to the data, a new latitudinal gradient G_θ^1 as the slope and the radial gradient G_r^1 as the intercept with the X -axis are found.

Figure 10 displays in the two left panels the radial and latitudinal gradients as a function of iteration steps. As starting conditions we took two physical and two non-physical extreme cases:

1. A large radial and negative latitudinal gradient (red curve). This case would have been the one expected for the current $A < 0$ -solar magnetic epoch (Cummings et al., 1987; McDonald et al., 1997a).
2. A small radial but a positive latitudinal gradient (blue curve). This case would be the one expected for an $A < 0$ -solar magnetic epoch (Heber et al., 2008).
3. A large radial and positive latitudinal gradient (black curve).
4. A small radial and negative latitudinal gradient (magenta curve).

The iterations stop when the gradients become stable within 0.002% from one step to the next. The minimization is performed using the code MINUIT (James and Roos, 1975).

Acknowledgements. The ULYSSES/KET project is supported under grant No. 50 OC 0902 and SUA 07/13 by the German Bundesministerium für Wirtschaft through the Deutsches Zentrum für

Luft- und Raumfahrt (DLR). The PAMELA mission is sponsored by the Italian National Institute of Nuclear Physics (INFN), the Italian Space Agency (ASI), the Russian Space Agency (Roskosmos), the Russian Academy of Science, the Deutsches Zentrum für Luft- und Raumfahrt (DLR), the Swedish National Space Board (SNSB) and the Swedish Research Council (VR). The German - Italian collaboration has been supported by the Deutsche Forschungsgemeinschaft under grant HE3279/11-1. This work profited from the discussions with the participants of the ISSI workshop “Cosmic Rays in the Heliosphere II”.

†PAMELA Collaboration

O. Adriani^{1,2}, G. C. Barbarino^{3,4}, G. A. Bazilevskaya⁵, R. Bellotti^{6,7}, M. Boezio⁸, E. A. Bogomolov⁹, L. Bonechi^{1,2}, M. Bongi², V. Bonvicini⁸, S. Borisov^{10,11,12}, S. Bottai², A. Bruno^{6,7}, F. Cafagna⁷, D. Campana⁴, R. Carbone^{4,11}, P. Carlson¹³, M. Casolino¹⁰, G. Castellini¹⁴, L. Consiglio⁴, M. P. De Pascale^{10,11}, C. De Santis^{10,11}, N. De Simone^{10,11}, V. Di Felice^{10,11}, A. M. Galper¹², W. Gillard¹³, L. Grishantseva¹², P. Hofverberg¹³, G. Jerse^{8,15}, A. V. Karelin¹², S. V. Koldashov¹², S. Y. Krutkov⁹, A. N. Kvashnin⁵, A. Leonov¹², V. Malvezzi¹⁰, L. Marcelli¹⁰, M. Martucci^{10,11}, A. G. Mayorov¹², W. Menn¹⁶, V. V. Mikhailov¹², E. Mocchiutti⁸, A. Monaco^{6,7}, N. Mori², N. Nikonov^{9,10,11}, G. Osteria⁴, F. Palma^{10,11}, P. Papini², M. Pearce¹³, P. Picozza^{10,11}, C. Pizzolotto⁸, M. Ricci¹⁷, S. B. Ricciarini², L. Rossetto¹³, M. Simon¹⁶, R. Sparvoli^{10,11}, P. Spillantini^{1,2}, Y. I. Stozhkov⁵, A. Vacchi⁸, E. Vannuccini², G. Vasilyev⁹, S. A. Voronov¹², J. Wu^{13,*}, Y. T. Yurkin¹², G. Zampa⁸, N. Zampa⁸, V. G. Zverev¹²

¹University of Florence, Department of Physics, I-50019 Sesto Fiorentino, Florence, Italy

²INFN, Sezione di Florence, I-50019 Sesto Fiorentino, Florence, Italy

³University of Naples “Federico II”, Department of Physics, I-80126 Naples, Italy

⁴INFN, Sezione di Naples, I-80126 Naples, Italy

⁵Lebedev Physical Institute, RU-119991, Moscow, Russia

⁶University of Bari, Department of Physics, I-70126 Bari, Italy

⁷INFN, Sezione di Bari, I-70126 Bari, Italy

⁸INFN, Sezione di Trieste, I-34149 Trieste, Italy

⁹Ioffe Physical Technical Institute, RU-194021 St. Petersburg, Russia

¹⁰INFN, Sezione di Rome “Tor Vergata”, I-00133 Rome, Italy

¹¹University of Rome “Tor Vergata”, Department of Physics, I-00133 Rome, Italy

¹²Moscow Engineering and Physics Institute, RU-11540 Moscow, Russia

¹³KTH, Department of Physics, and the Oskar Klein Centre for Cosmoparticle Physics
AlbaNova University Centre, SE-10691 Stockholm, Sweden

¹⁴IFAC, I-50019 Sesto Fiorentino, Florence, Italy

¹⁵University of Trieste, Department of Physics, I-34147 Trieste, Italy

¹⁶Universität Siegen, Department of Physics, D-57068 Siegen, Germany

¹⁷INFN, Laboratori Nazionali di Frascati, Via Enrico Fermi 40, I-00044 Frascati, Italy

*On leave from School of Mathematics and Physics, China University of Geosciences, CN-430074 Wuhan, China

Edited by: R. Vainio

Reviewed by: two anonymous referees

References

- Burger, R. A., Potgieter, M. S., and Heber, B.: Rigidity dependence of cosmic ray proton latitudinal gradients measured by the Ulysses spacecraft: Implications for the diffusion tensor, *J. Geophys. Res.*, 105, 27 447–27 456, doi:10.1029/2000JA000153, 2000.
- Casolino, M., Picozza, P., Altamura, F., Basili, A., De Simone, N., Di Felice, V., Pascale, M. D., Marcelli, L., Minori, M., Nagni, M., Sparvoli, R., Galper, A., Mikhailov, V., Runtso, M., Voronov, S., Yurkin, Y., Zverev, V., Castellini, G., Adriani, O., Bonechi, L., Bongi, M., Taddei, E., Vannuccini, E., Fedele, D., Papini, P., Ricciarini, S., Spillantini, P., Ambriola, M., Cafagna, F., Marzo, C. D., Barbarino, G., Campana, D., Rosa, G. D., Osteria, G., Russo, S., Bazilevskaja, G., Kvashnin, A., Maksumov, O., Misin, S., Stozhkov, Y., Bogomolov, E., Krutkov, S., Nikonov, N., Bonvicini, V., Boezio, M., Lundquist, J., Mocchiutti, E., Vacchi, A., Zampa, G., Zampa, N., Bongiorno, L., Ricci, M., Carlson, P., Hofverberg, P., Lund, J., Orsi, S., Pearce, M., Menn, W., and Simon, M.: Launch of the space experiment PAMELA, *Adv. Space Res.*, 42, 455–466, doi:10.1016/j.asr.2007.07.023, <http://www.sciencedirect.com/science/article/B6V3S-4P9625D-1/2/7b49861564f9fa0f239fb6523df2f03a>, 2008.
- Cummings, A. C., Stone, E. C., and Webber, W. R.: Latitudinal and radial gradients of anomalous and galactic cosmic rays in the outer heliosphere, *Geophys. Res. Lett.*, 14, 174–177, 1987.
- Eadie, W. T., Drijard, D., James, F. E., Roos, M., and Sadoulet, B.: *Statistical methods in experimental physics*, North-Holland, Amsterdam, 1971.
- Ferreira, S. E. S. and Potgieter, M. S.: Long-Term Cosmic-Ray Modulation in the Heliosphere, *Astrophys. J.*, 603, 744–752, doi:10.1086/381649, 2004.
- Ferreira, S. E. S., Potgieter, M. S., Heber, B., and Fichtner, H.: Charge-sign dependent modulation in the heliosphere over a 22-year cycle, *Ann. Geophys.*, 21, 1359–1366, 2003.
- Fujii, Z. and McDonald, F. B.: The radial intensity gradients of galactic and anomalous cosmic rays, *Adv. Space Res.*, 23, 437–441, doi:10.1016/S0273-1177(99)00101-5, 1999.
- Gieseler, J., De Simone, N., Heber, B., and Di Felice, V.: The response function of the Kiel Electron Telescope, re-investigated, *Adv. Space Res.*, p. in preparation, 2010.
- Heber, B., Dröge, W., Ferrando, P., Haasbroek, L., Kunow, H., Müller-Mellin, R., Paizis, C., Potgieter, M., Raviart, A., and Wibberenz, G.: Spatial variation of > 40 MeV/n nuclei fluxes observed during Ulysses rapid latitude scan, *Astron. Astrophys.*, 316, 538–546, 1996a.

- Heber, B., Dröge, W., Kunow, H., Müller-Mellin, R., Wibberenz, G., Ferrando, P., Raviart, A., and Paizis, C.: Spatial variation of > 106 MeV proton fluxes observed during the Ulysses rapid latitude scan: Ulysses COSPIN/KET results, *Geophys. Res. Lett.*, 23, 1513–1516, 1996b.
- Heber, B., Ferrando, P., Raviart, A., Wibberenz, G., Müller-Mellin, R., Kunow, H., Sierks, H., Bothmer, V., Posner, A., Paizis, C., and Potgieter, M. S.: Differences in the temporal variation of galactic cosmic ray electrons and protons: Implications from Ulysses at solar minimum, *Geophys. Res. Lett.*, 26, 2133–2136, 1999.
- Heber, B., Gieseler, J., Dunzlaff, P., Gomez-Herrero, R., Müller-Mellin, R., Mewaldt, R., Potgieter, M. S., and Ferreira, S.: Latitudinal gradients of galactic cosmic rays during the 2007 solar minimum, *Astrophys. J.*, 1, doi:10.1086/592596, 2008.
- Heber, B., Kopp, A., Gieseler, J., Müller-Mellin, R., Fichtner, H., Scherer, K., Potgieter, M. S., and Ferreira, S. E. S.: Modulation of Galactic Cosmic Ray Protons and Electrons During an Unusual Solar Minimum, *Astrophys. J.*, 699, 1956–1963, doi:10.1088/0004-637X/699/2/1956, 2009.
- James, F. and Roos, M.: Minuit - a system for function minimization and analysis of the parameter errors and correlations, *Computer Physics Communications*, 10, 343–367, doi:10.1016/0010-4655(75)90039-9 <http://www.sciencedirect.com/science/article/B6TJ5-46FPXJ7-2C/2/58a665cfce07e122711a859fef69c955>, 1975.
- Jokipii, J. R., Levy, E. H., and Hubbard, W. B.: Effects of particle drift on cosmic ray transport, I. General properties, application to solar modulation, *Astrophys. J.*, 213, 861–868, 1977.
- McComas, D. J., Ebert, R. W., Elliott, H. A., Goldstein, B. E., Gosling, J. T., Schwadron, N. A., and Skoug, R. M.: Weaker solar wind from the polar coronal holes and the whole Sun, *Geophys. Res. Lett.*, 35, 18103, doi:10.1029/2008GL034896, 2008.
- McDonald, F. B., Ferrando, P., Heber, B., Kunow, H., McGuire, R., Müller-Mellin, R., Paizis, C., Raviart, A., and Wibberenz, G.: A comparative study of cosmic ray radial and latitudinal gradients in the inner and outer heliosphere, *J. Geophys. Res.*, 102, 4643–4652, doi:10.1029/96JA03673, 1997a.
- McDonald, F. B., Ferrando, P., Heber, B., Kunow, H., McGuire, R., Müller-Mellin, R., Paizis, C., Raviart, A., and Wibberenz, G.: A comparative study of cosmic ray radial and latitudinal gradients in the inner and outer heliosphere, *J. Geophys. Res.*, 102, 4643–4652, doi:10.1029/96JA03673, 1997b.
- McKibben, R. B.: Reanalysis and confirmation of positive latitude gradients for anomalous helium and Galactic cosmic rays measured in 1975–1976 with Pioneer II, *J. Geophys. Res.*, 94, 17021–17033, 1989.
- Minnie, J., Bieber, J. W., Matthaeus, W. H., and Burger, R. A.: On the Ability of Different Diffusion Theories to Account for Directly Simulated Diffusion Coefficients, *Astrophys. J.*, 663, 1049–1054, doi:10.1086/518765, 2007.
- Picozza, P., Galper, A. M., Castellini, G., Adriani, O., Altamura, F., Ambriola, M., Barbarino, G. C., Basili, A., Bazilevskaia, G. A., Bencardino, R., et al.: PAMELA-A payload for antimatter matter exploration and light-nuclei astrophysics, *Astroparticle Physics*, 27, 296315, 2007.
- Potgieter, M. S., Ferreira, S. E. S., and Burger, R.: Modulation of cosmic rays in the heliosphere over 11 and 22 year cycles: a modelling perspective, *Adv. Space Res.*, 27, 481–492, 2001.
- Shalchi, A., Li, G., and Zank, G. P.: Analytic forms of the perpendicular cosmic ray diffusion coefficient for an arbitrary turbulence spectrum and applications on transport of Galactic protons and acceleration at interplanetary shocks, *Astrophys. Space Sci.*, 325, 99–111, doi:10.1007/s10509-009-0168-6, 2010.
- Simpson, J., Anglin, J., Barlogh, A., Bercovitch, M., Bouman, J., Budzinski, E., Burrows, J., Carvell, R., Connell, J., Ducros, R., Ferrando, P., Firth, J., Garcia-Munoz, M., Henrion, J., Hynds, R., Iwers, B., Jacquet, R., Kunow, H., Lentz, G., Marsden, R., McKibben, R., Müller-Mellin, R., Page, D., Perkins, M., Raviart, A., Sanderson, T., Sierks, H., Treguer, L., Tuzzolino, A., Wenzel, K.-P., and Wibberenz, G.: The Ulysses Cosmic-Ray and Solar Particle Investigation, *Astron. Astrophys. Suppl.*, 92, 365–399, 1992.
- Simpson, J. A., Zhang, M., and Bame, S.: A Solar Polar North-South Asymmetry for Cosmic-Ray Propagation in the Heliosphere: The ULYSSES Pole-to-Pole Rapid Transit, *Astrophys. J. Lett.*, 465, L69, 1996.
- Smith, E. J. and Balogh, A.: Decrease in heliospheric magnetic flux in this solar minimum: Recent Ulysses magnetic field observations, *Geophys. Res. Lett.*, 35, 22 103, doi:10.1029/2008GL035345, 2008.